

# A Price-Based Strategy to Coordinate Electric Springs for Demand Side Management in Microgrids

Darwin A. Quijano, Morteza Vahid-Ghavidel, *Student Member, IEEE*, Mohammad Sadegh Javadi, *Senior Member, IEEE*, Antonio Padilha-Feltrin, *Senior Member, IEEE* and João P. S. Catalão, *Fellow, IEEE*.

**Abstract**—Electric springs (ESs) have proven effective for integrating renewable generation into power systems. An ES connected in series with a non-critical load forms a smart load whose consumption can be dynamically controlled for voltage regulation and demand side management. In most existing applications, smart loads have been devoted to providing services to the grid without accounting for their own interests. The novelty of this paper is to propose a price-based strategy to coordinate the operation of multiple ESs in microgrids. Smart loads consisting of ESs connected to electric water heaters are modeled as rational agents that locally optimize their own objectives by adjusting their consumption schedules in response to price/control signals. Such signals are determined at the microgrid central controller (MGCC) when solving the microgrid operation scheduling problem formulated to minimize the microgrid operation cost taking into account the smart loads' consumption schedules. An iterative optimization algorithm determines the equilibrium between the microgrid and smart loads' objectives requiring only the exchange of price/control signals and power schedules between the local controllers and the MGCC. Case studies show the effectiveness of the proposed strategy to economically benefit both the microgrid and smart loads when scheduling their operation.

**Index Terms**—Distributed optimization, electric spring, microgrid, renewable energy, smart pricing.

## NOMENCLATURE

### Indices and sets:

$i, ij, t$  Indices for bus, line segment, time interval;  
 $\Omega_b, \Omega_l, \Omega_t$  Sets of buses, line segments, time intervals.

### Parameters:

$P_i^{g,\min}, P_i^{g,\max}$  Minimum and maximum black power outputs of dispatchable DG;  
 $R_i^{\max}$  Maximum ramping of dispatchable DG;  
 $S_i$  Rated capacity of dispatchable DG;  
 $\alpha_i^g, \beta_i^g, \nu_i^g$  Coefficients of cost function of dispatchable DG;  
 $\omega_t$  Normalized wind power;  
 $P_i^{ic}$  Installed capacity of wind-based DG;

This work was supported by São Paulo Research Foundation (FAPESP) under grants: 2018/06451-8, 2020/12401-3 and 2015/21972-6, by CNPq under grant: 310299/2020-9, and by CAPES (code finance 001).

D.A. Quijano is with Universidade Estadual Paulista–UNESP, Ilha Solteira 15385-000, Brazil, and INESC TEC, 4200-465, Porto, Portugal (e-mail: alexisqr@yahoo.es).

M.S. Javadi is with INESC TEC, 4200-465, Porto, Portugal (e-mail: msjavadi@gmail.com)

A. Padilha-Feltrin is with Universidade Estadual Paulista–UNESP, Ilha Solteira 15385-000, Brazil (e-mail: antonio.padilha-feltrin@unesp.br).

M. Vahid-Ghavidel and J.P.S. Catalão are with the Faculty of Engineering of the University of Porto (FEUP) and INESC TEC, 4200-465, Porto, Portugal (e-mail: mv.ghavidel@gmail.com; catalao@fe.up.pt)

$\alpha_i^w$  Coefficient of cost function of wind spillage;  
 $\hat{P}_{i,t}^{cl}, \hat{Q}_{i,t}^{cl}$  Active and reactive CL powers;  
 $\alpha_i^{cl}$  Coefficient of cost function of CL shedding  
 $R_i^{nc}$  Resistance of the EWH heating element;  
 $T^l, T^u, T^a$  Cold water temperature, hot water temperature and ambient temperature;  
 $c, m$  Specific heat capacity and density of water;  
 $\Delta t$  Duration of the time interval;  
 $W_{i,t}$  Rate of hot water draw from the EWH;  
 $\eta$  Efficiency of the EWH heating element;  
 $P_i^{alu}$  Maximum heat loss of the EWH;  
 $E_i^a, E_i^{\max}, E_i^{\min}$  Thermal energy stored in the EWH when it is full of water at ambient temperature, hot water and cold water;  
 $L_i$  Total volume of the EWH;  
 $\alpha_i^{nc}$  Coefficient of cost function of smart load;  
 $\delta_i$  Parameter that indicates the minimum acceptable state of thermal charge of EWH;  
 $SC_i^{\max}$  Maximum state of thermal charge of EWH;  
 $r_{ij}, x_{ij}$  Resistance and reactance in line segments;  
 $\alpha_i^p$  Coefficient of cost function of energy losses;  
 $V_i^{\min}, V_i^{\max}$  Minimum and maximum bus voltage limits;  
 $V^n$  Nominal voltage;  
 $C_1, C_2, C_3$  Coefficient matrices for SDP relaxation;  
 $\mu_{i,t}^k, \lambda_{i,t}^k$  Lagrangian multipliers in the corrector step;  
 $\hat{\mu}_{i,t}^k, \hat{\lambda}_{i,t}^k$  Lagrangian multipliers in the predictor step;  
 $\gamma$  Positive parameter.

### Functions:

$C^g(P_{i,t}^g)$  Cost function of dispatchable DG;  
 $C^w(P_{i,t}^w)$  Cost function of wind spillage;  
 $C^{cl}(P_{i,t}^{cl})$  Cost function of CL shedding;  
 $C^{nc}(SC_{i,t})$  Cost function of smart load.

### Variables:

$P_{i,t}^g, Q_{i,t}^g$  Active and reactive power outputs of dispatchable DG;  
 $P_{i,t}^w$  Active power output of wind-based DG;  
 $P_{i,t}^{cl}, Q_{i,t}^{cl}$  Active and reactive powers of CL;  
 $SC_{i,t}$  State of thermal charge of EWH;  
 $I_{ij,t}^{sqr}$  Magnitude squared of current in line segments;  
 $I_{i,t}^{nc}$  Magnitude of NCL current;  
 $V_{i,t}^{nc}$  Magnitude of NCL voltage;  
 $V_{i,t}^{es}$  Magnitude of ES voltage;  
 $V_{i,t}^{sqr}$  Magnitude squared of bus voltage;  
 $P_{i,t}^{nc}$  Active power supplied to the EWH;  
 $Q_{i,t}^{es}$  Reactive power injected by the ES;  
 $E_{i,t}$  Thermal energy stored in the EWH;

$E_{i,t}^l, E_{i,t}^u$	Thermal energy stored in the lower and upper water layers of the EWH;
$L_{i,t}^l, L_{i,t}^u$	Volume of the lower and upper water layers in the EWH;
$P_{i,t}^{al}, P_{i,t}^{au}$	Heat loss from the lower and upper water layers in the EWH;
$P_{i,t}^{lu}$	Thermal conduction between the lower and upper water layers in the EWH;
$P_{i,t}^a$	Total heat loss from the EWH;
$SC_{i,t}$	State of thermal charge of the EWH;
$P_{ij,t}, Q_{ij,t}$	Active and reactive power flows in line segments;
$X_{i,t}$	Variable matrix for SDP relaxation.

## I. INTRODUCTION

Electric spring (ES) is a novel concept devised to integrate renewable energy sources (RESs) into power systems. Physically, it consists of a power inverter that is connected in series with a non-critical load (NCL) to regulate its consumption [1]. In this definition, NCLs are those that tolerate a wide range of voltage variations, as opposed to critical loads (CLs) which require a tightly regulated voltage. The operation principle of the series arrangement ES-NCL (usually referred to as smart load) consists in controlling the ES voltage output to induce a change in the voltage supplied to the NCL which in turn results in a change in its consumption. When deployed in distribution systems, ESs can be used for the NCLs consumption to follow the variation of the RES-based DG power production, providing regulation of bus voltages and power flows.

After the proof of concept of ES was presented in [1], several studies have investigated different applications and control strategies for ESs. Some of these studies have demonstrated ES applications considering a single and locally-controlled ES installed in a system with RES-based DG power supply. For example, in [2], an ES is used to damp electric oscillations and provide critical loads (CLs) with a well-regulated voltage. In [3], besides providing voltage stabilization, the ES is also used for frequency stabilization in a microgrid. A control scheme for an ES to provide power and voltage stability and power factor correction is proposed in [4]. The authors of [5] demonstrated the effectiveness of ESs in reducing energy storage requirements in power grids. In [6], an integrated configuration of ES and a photovoltaic (PV) system is used for dynamic supply-demand balance. The utilization of an ES to provide constant power to a load with varying impedance is investigated in [7].

Although experiments with a single ES are useful to demonstrate possible applications, the full potential of ESs will be realized only if they are widely dispersed in the distribution systems. For this reason, it becomes necessary to develop control strategies to coordinate the operation of multiple distributed ESs. This was addressed in [8] through a droop control method applied to support and stabilize the bus voltage levels. The discrete consensus algorithm is proposed in [9] to solve the coordination control of multiple ESs for bus voltage stability. In [10], ESs are centrally coordinated through a predictive control with the aim of reducing the energy losses in a microgrid. In [11], an optimization model

applied to minimize the bus voltage deviations in a transactive energy system is proposed. The authors of [12] propose an optimization model to determine the best locations and capacities of ESs to minimize the total bus voltage deviations in distribution systems.

The types of NCLs suitable for operation with ESs (e.g., electric water heaters (EWHs), refrigerators and lighting systems) are non-critical in the sense of their high tolerance to voltage variations. However, it is still necessary to consider their physical constraints and ensure customer comfort when they participate in demand-side management, which has not been addressed in the above-discussed works [1]–[12]. In [13], a model of a central ice-thermal storage embedded into a building energy system is used to describe an NCL whose consumption is controlled by an ES to provide bus voltage regulation and dynamic supply-demand balance in a power grid; however, this study does not consider the coordination of multiple ESs. Chen *et al.* [14] model the dynamics of the thermal cycle of EWHs within a distributed control based on a dynamic consensus control algorithm applied to coordinate multiple ESs for overvoltage prevention. The authors of [15] use a realistic model of water heater system to describe NCLs, and propose a model predictive control to centrally minimize the operation cost of a microgrid considering the ES operation. Although the formulation is applicable to the case of multiple ESs, its performance is evaluated in a microgrid with a single ES. Zhang *et al.* [16] propose a scheduling strategy to control the power consumption of air conditioners installed with ESs to smooth the peak-valley difference on the distribution system.

Smart loads participating in demand-side management may belong to different entities and they may want to optimize their own operation cost and customers comfort, and preserve their information (e.g., consumption preferences and constraints) private [17]. Smart pricing is known as one of the most common mechanisms that can be used to indirectly coordinate the operation of flexible loads [18], [19]. When implemented, loads respond to price signals by selecting the consumption patterns that achieve the best trade-off between cost and comfort. Nevertheless, to the best of the authors' knowledge, smart pricing has not yet been investigated in applications with ESs. The distributed control methods of ESs proposed in [8], [9], [14] remove the need for the smart loads to share their information; however, they do not optimize the operation cost of the smart loads and the power grid.

To fill the void existing in the literature, this paper addresses the problem of coordinating the operation of multiple ESs through a smart pricing strategy. This strategy is designed for the day-ahead operation scheduling of islanded microgrids that seek to minimize their operation cost taking advantage of the flexibility of smart loads. A microgrid can operate in islanded mode due to disturbances in the main grid. In addition, always-islanded microgrids (referred to as isolated microgrids) have been proposed as a solution to provide energy to remote communities that cannot be connected to the main grid due to technical and/or economical limitations [20]–[22]. The operation scheduling of a microgrid involves coordinating the dispatch of the different distributed energy

resources (DERs) and loads based on predictions of energy production and consumption [23]. In this work, smart loads consist of ESs connected to EWHs, which are modeled taking into account their electric and thermal constraints and the hot water demand. By smartly choosing the price/control signals broadcast to smart loads it is intended that they respond by adjusting their power schedules in a way that simultaneously optimizes their own objectives and the objective of the microgrid.

Initially, the microgrid operation scheduling problem is formulated for a centralized solution as an optimal power flow that seeks to minimize the microgrid operation cost and the discomfort of customers while maintaining adequate bus voltage levels. The microgrid operation cost is given by the cost of dispatchable generation, cost of energy not supplied from RES, cost of CL shedding and cost of energy losses. This formulation corresponds to a centralized approach in which the dispatch decisions of all DERs and loads (including smart loads) are computed by the microgrid central controller (MGCC). The predictor-corrector proximal multiplier (PCPM) algorithm [24], [25] is then applied to decouple the optimization of the smart loads and compute the ESs voltage references and EWHs power schedules in a distributed way by the local controllers. To apply the PCPM algorithm, the non-convex constraints of the power flows and ESs are first convexified. Through this approach, price/control signals are determined at the MGCC when scheduling the power flows in the microgrid. Such signals are sent to the ESs local controllers, which in turn solve their corresponding optimization problems to find the optimal smart loads' active and reactive power schedules. The problem is iteratively solved while updating the price/control signals and smart loads' active and reactive power schedules until finding the equilibrium between the microgrid and smart load objectives.

The major contributions of this paper are listed as follows:

- Smart loads composed of ESs connected to EWHs are modeled as rational agents that adjust their power schedules in response to price/control signals to optimize their own operation cost and customer comfort. The price/control signals are obtained from the microgrid operation scheduling as those that minimize the microgrid operation cost when smart loads provide flexibility.
- An optimization algorithm that decouples the microgrid and smart loads scheduling problems to distribute the computations between the MGCC and local controllers. This algorithm iteratively finds an equilibrium between the microgrid and smart loads objectives, requiring only the exchange of price/control signals and power schedules between the MGCC and the local controllers.
- Multiple ESs are applied to minimize the operation cost of microgrids and for voltage regulation. To the best of the authors' knowledge, this is the first time the operation of multiple ESs is coordinated through a price-based strategy for these applications.
- A semidefinite programming (SDP)-based convex relaxation of the non-linear equations that describe the ES operation. By convexifying the non-linear equations it is possible to decompose the microgrid operation scheduling problem.

## II. OPTIMIZATION MODEL FOR THE MICROGRID

This section presents the formulation of the microgrid operation scheduling problem for a centralized solution. The formulation includes the constraints and cost functions of dispatchable DG, RES-based DG, CLs and smart loads, and power the flow equations.

### A. Objective function

Costs of dispatchable DG, energy not supplied from RES-based DG, CLs shedding, state of thermal charge (SOTC) of EWHs and energy losses are considered in the objective function as follows:

$$\min \sum_{t \in \Omega_t} \left( \sum_{i \in \Omega_b} \left( C^g (P_{i,t}^g) + C^w (P_{i,t}^w) + C^{cl} (P_{i,t}^{cl}) + C^{nc} (SC_{i,t}) \right) + \alpha_i^b \sum_{ij \in \Omega_l} r_{ij} I_{ij}^{sqr} \right). \quad (1)$$

Each term of (1) is defined in the following subsections that describe the models of the microgrid components.

### B. DG model

The microgrid energy consumption is supplied by RES-based DG and dispatchable DG (diesel generators). Each of these generation technologies is modeled taking into account the availability of the primary energy source. Other types of DG can be easily integrated into the model without affecting the validity of the analysis.

1) *Dispatchable DG*: Diesel generators are dispatchable and their power output can be varied between a range taking into account their ramping ability according to the following constraints:

$$P_i^{g,\min} \leq P_{i,t}^g \leq P_i^{g,\max}, \quad \forall(i, t), \quad (2)$$

$$-R_i^{\max} \leq P_{i,t}^g - P_{i,t-1}^g \leq R_i^{\max}, \quad \forall(i, t), \quad (3)$$

where, (2) limits the diesel generators power output to minimum and maximum values, and (3) limits the ramping ability of diesel generators to a maximum value. The maximum reactive power that a diesel generator can supply is determined by its capability curve defined as follows:

$$P_{i,t}^{g^2} + Q_{i,t}^{g^2} \leq S_i^2, \quad \forall(i, t). \quad (4)$$

A quadratic model is used to describe the cost function of the diesel generators as follows:

$$C^g (P_{i,t}^g) = \alpha_i^g P_{i,t}^{g^2} + \beta_i^g P_{i,t}^g + v_i^g, \quad \forall(i, t). \quad (5)$$

2) *Wind-based DG*: Wind-based DG is non-dispatchable because its power availability is subject to the variability of the wind speed. The power output of wind-based DG is constrained as follows:

$$0 \leq P_{i,t}^w \leq \omega_t^w P_i^{ic}, \quad \forall(i, t), \quad (6)$$

where the term  $\omega_t^w P_i^{ic}$  represents the maximum power that the wind-based DG at bus  $i$  can generate at time interval  $t$ . The cost function of the wind-based DG penalizes the wind spillage as follows:

$$C^w (P_{i,t}^w) = \alpha_i^w (\omega_t^w P_i^{ic} - P_{i,t}^w), \quad \forall(i, t). \quad (7)$$

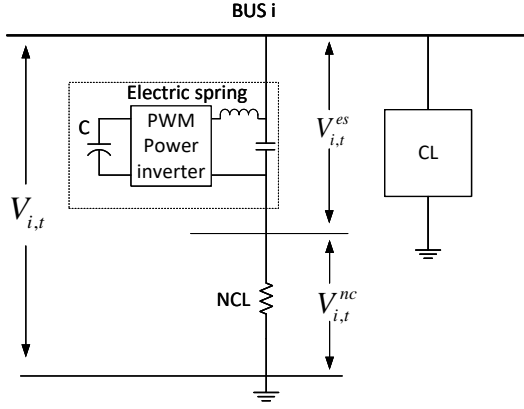


Fig. 1. Diagram of smart load configuration.

### C. Critical loads

Critical loads are those that require a tightly regulated voltage and reliable power supply. The active and reactive powers supplied to CLs are constrained as follows:

$$0 \leq P_{i,t}^{cl} \leq \hat{P}_{i,t}^{cl}, \quad \forall(i, t), \quad (8)$$

$$0 \leq Q_{i,t}^{cl} \leq \hat{Q}_{i,t}^{cl}, \quad \forall(i, t). \quad (9)$$

The cost function of CLs penalizes the load shedding as follows:

$$C^{cl}(P_{i,t}^{cl}) = \alpha_i^{cl} (\hat{P}_i^{cl} - P_{i,t}^{cl}), \quad \forall(i, t). \quad (10)$$

### D. Smart loads model

In this work, a smart load consists of an ES connected in series with a NCL. A diagram of the configuration of an smart load connected in parallel with a pure resistive NCL is shown in Fig. 1. By generating a voltage  $V_{i,t}^{es}$  in parallel to the NCL, the ES is capable of regulating the voltage  $V_{i,t}^{nc}$  and the power  $P_{i,t}^{nc}$  supplied to the NCL.

1) *Electric spring*: The proposed configuration considers an ES with reactive power control only, which not requires battery storage. This is the first generation of ES and consist of an inverter with a capacitor installed on the DC-link side and an inductor-capacitor (LC) filter on the ac side [1]. To ensure that the ES only exchanges reactive power, its output voltage must be controlled to remain perpendicular to the NCL current vector. The set of equations that describe the ES operation is represented as follows:

$$V_{i,t}^{nc2} + V_{i,t}^{es2} = V_{i,t}^{sqr}, \quad \forall(i, t), \quad (11)$$

$$P_{i,t}^{nc} = \frac{V_{i,t}^{nc2}}{R_i^{nc}}, \quad \forall(i, t), \quad (12)$$

$$Q_{i,t}^{es} = \frac{V_{i,t}^{es} V_{i,t}^{nc}}{R_i^{nc}}, \quad \forall(i, t), \quad (13)$$

$$0 \leq V_{i,t}^{es2} \leq V_{i,t}^{sqr}, \quad \forall(i, t), \quad (14)$$

where, (11) describes the relationship between the magnitudes of microgrid bus voltage, ES voltage and NCL voltage. Fig. 2 shows these voltages for the ES operating under inductive and capacitive modes when connected to a pure resistive NCL. Constraint (12) models the NCL active power as a function of the supplied voltage. The reactive power exchanged by the ES is expressed in (13) as the product between the ES voltage and

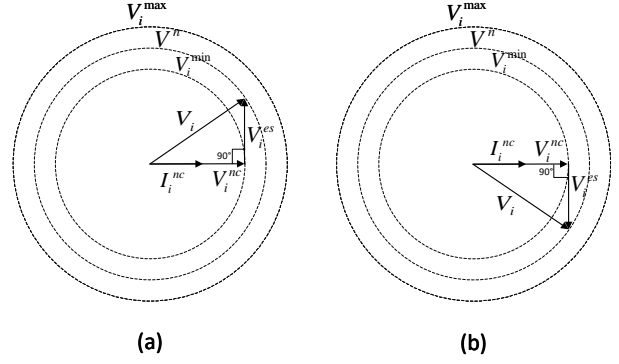


Fig. 2. Phasor diagram of electric spring operating under (a) inductive and (b) capacitive modes.

the NCL current. The ES voltage is constrained to be lower than the microgrid voltage in (14). In (13), it is assumed that  $V_{i,t}^{es}$  takes negative values for capacitive operation and positive values for inductive operation of the ES [15].

2) *Non-critical load*: The type of NCL considered in this work is the EWH, which is modeled taking into account its electric and thermal characteristics and the hot water consumption. A diagram of an EWH composed of a tank and two heating elements with their respective thermostats is shown in Fig. 3. To model the dynamics of the hot water usage and heating process, the water tank is vertically divided into three layers: a lower layer with cold water, an upper layer with hot water, and a mixing layer in between [14]. When hot water is drawn from the tank, cold water enters through an input located at the bottom of the tank. The cold water remains in the lower layer at the bottom of the tank because is denser than the hot water. Once is heated, the water moves to the upper layer. The mixing layer moves up and down depending on the content of hot water in the tank. For simplicity, in this model the thickness of the mixing layer is assumed zero. Further, the upper heating element is disregarded because, in practice, it is turned on only when the cold water layer reaches a critical level [14]. The total thermal energy stored in the tank is the sum of the energy stored in the lower and upper layers expressed as follows:

$$E_{i,t} = E_{i,t}^l + E_{i,t}^u = cmL_{i,t}^l T^l + cmL_{i,t}^u T^u, \quad \forall(i, t). \quad (15)$$

The change in the thermal energy stored in the lower and upper layers between two consecutive time intervals is given by

$$E_{i,t}^l = E_{i,t-1}^l + \Delta t (cmW_{i,t} T^l + \eta P_{i,t}^{nc} - P_{i,t}^{al} + P_{i,t}^{lu}), \quad \forall(i, t), \quad (16)$$

$$E_{i,t}^u = E_{i,t-1}^u - \Delta t (cmW_{i,t} T^u + P_{i,t}^{au} + P_{i,t}^{lu}), \quad \forall(i, t). \quad (17)$$

From (15)–(17) it is deduced the dynamic thermal energy balance equation that describes the change in the total thermal energy stored in the tank between two consecutive time intervals as follows:

$$E_{i,t} = E_{i,t-1} + \Delta t (\eta P_{i,t}^{nc} + cmW_{i,t} (T^l - T^u) - P_{i,t}^a), \quad \forall(i, t). \quad (18)$$

The heat loss from the water in the tank to the ambient air is calculated as follows [14]:

$$P_{i,t}^a = P_{i,t}^{al} + P_{i,t}^{au} = P_{i,t}^{al} \frac{E_{i,t} - E_i^a}{E_i^{max} - E_i^a}, \quad \forall(i, t), \quad (19)$$

where,  $E_i^a = cmL_i T^a$ ,  $E_i^{max} = cmL_i T^u$  and  $L_i = L_{i,t}^l + L_{i,t}^u$ .  $P_{i,t}^{al}$  is obtained from

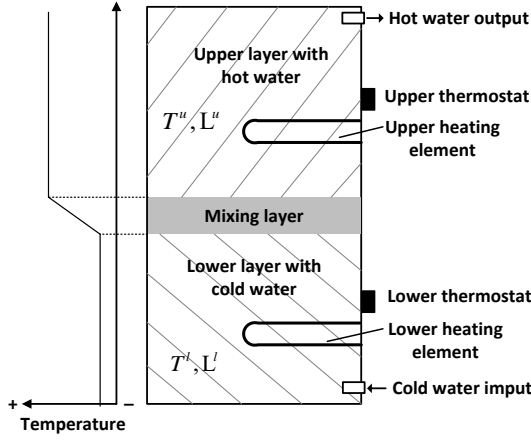


Fig. 3. Configuration and temperature profile of an EWH.

$$P_i^{alu} = cmL_i(T^u - T^a)/\tau, \quad \forall i, \quad (20)$$

where,  $\tau$  is a constant that indicates the time it takes the thermal losses to bring down the water temperature from  $T^u$  to  $T^a$ , and in this work is set to 120 h [26]. The thermal energy stored in the tank is limited to lower and upper limits as follows:

$$E_i^{min} \leq E_{i,t} \leq E_i^{max}, \quad \forall(i, t), \quad (21)$$

where,  $E^{min} = cmL_iT^l$ . The SOTC used to indicate the level of thermal energy stored in the EWH available for usage is defined as follows:

$$SC_{i,t} = \frac{E_{i,t} - E_i^{min}}{E_i^{max} - E_i^{min}}, \quad \forall(i, t), \quad (22)$$

The cost function of the smart load penalizes SOTCs lower than a specified limit as follows:

$$C^{mc}(SC_{i,t}) = \alpha_i^{nc} (\min(SC_{i,t} - \delta_i SC_i^{max}, 0))^2, \quad \forall(i, t). \quad (23)$$

This function is analogous to the cost function used to penalize deep discharging in battery energy storage systems and was taken from [19]. In this way, it is pretended to ensure the availability of hot water at any moment and minimize the discomfort of the users when the EWHs participates in DSM.

### E. Power flow equations

The complex power flows and voltages at the microgrid buses are described by the DistFlow equations represented as follows [27]:

$$\sum_{ij \in \Omega_l} P_{ij,t} - P_{hi,t} + r_{ki} I_{hi}^{sqr} + p_{i,t} = 0, \quad \forall(i, t), \quad (24)$$

$$\sum_{ij \in \Omega_l} Q_{ij,t} - Q_{hi,t} + x_{ki} I_{hi}^{sqr} + q_{i,t} = 0, \quad \forall(i, t), \quad (25)$$

$$p_{i,t} = P_{i,t}^{cl} + P_{i,t}^{nc} - P_{i,t}^g - P_{i,t}^w, \quad \forall(i, t), \quad (26)$$

$$q_{i,t} = Q_{i,t}^{cl} + Q_{i,t}^{es} - Q_{i,t}^g, \quad \forall(i, t), \quad (27)$$

$$V_{j,t}^{sqr} = V_{i,t}^{sqr} - 2(r_{ij} P_{ij,t} + x_{ij} Q_{ij,t}) + (r_{ij}^2 + x_{ij}^2) I_{ij,t}^{sqr}, \quad \forall(i, t), \quad (28)$$

$$I_{ij,t}^{sqr} = \frac{P_{ij,t}^2 + Q_{ij,t}^2}{V_{i,t}^{sqr}}, \quad \forall(i, t), \quad (29)$$

where  $h$  is the node upstream node  $i$  and  $j|ij \in \Omega_l$  is the set of nodes downstream node  $i$ , considering a radial topology of the

microgrid. At each node, (26) and (27) calculate the net active and reactive power injections subtracting the generation from the sum of the CL and NCL demands. If there is no generator or load at a given node  $i$ , the corresponding variables of active and reactive power becomes zero. Bus voltages are limited to the minimum and maximum values as follows:

$$V_{i,t}^{min} \leq V_{i,t}^{sqr} \leq V_{i,t}^{max}, \quad \forall(i, t). \quad (30)$$

Variables  $V_{i,t}^{sqr}$  and  $I_{ij,t}^{sqr}$  replace the quadratic terms  $V_{ij,t}^2$  and  $I_{ij,t}^2$  in the model. Therefore, the only nonlinear expression in the power flow equations corresponds to constraint (29).

### III. MODEL CONVEXIFICATION

The above optimization problem, given by the objective function (1) subject to constraints (2)–(14) and (18)–(30), is nonconvex due to 1) the quadratic equality constraint (29) that describe the magnitude squared of the line current in the power flow equations, and 2) the quadratic equality constraints (11)–(13) that model the ES operation. The non-convexity makes this problem NP-hard to solve and also makes challenging the application of a decomposition algorithm. Therefore, a convex relaxation for the problem is applied. Constraint (28) is convexified by relaxing the equality as follows:

$$I_{ij,t}^{sqr} \geq \frac{P_{ij,t}^2 + Q_{ij,t}^2}{V_{ij,t}^{sqr}}, \quad \forall(i, t). \quad (31)$$

Sufficient conditions for this relaxation to be exact is that the bus voltage is kept around the nominal value and that the power injection at each bus is not too large [28].

For the convexification of the ES constraints (11)–(13), a SDP relaxation [29] is applied as follows:

$$C_1 \bullet X_{i,t} - V_{i,t}^{sqr} = 0, \quad \forall(i, t), \quad (32)$$

$$C_2 \bullet X_{i,t} - P_{i,t}^{nc} = 0, \quad \forall(i, t), \quad (33)$$

$$C_3 \bullet X_{i,t} - Q_{i,t}^{es} = 0, \quad \forall(i, t), \quad (34)$$

$$X_{i,t} \succeq 0, \quad \forall(i, t), \quad (35)$$

where,  $C_n$  ( $n = 1, 2, 3$ ) are  $2 \times 2$  coefficient matrices and  $X_{i,t} := (X_{i,t,k,l}, k = 1, 2, l = 1, 2)$  is a  $2 \times 2$  symmetric matrix variable defined for each bus  $i$  and time interval  $t$ . In addition,  $C_n \bullet X_{i,t} := \sum_{k=1}^2 \sum_{l=1}^2 C_{n,k,l} X_{i,t,k,l}$ . Constraint (35) indicates that the matrix variable  $X_{i,t}$  must be positive semidefinite. The coefficient matrices  $C_n$  ( $n = 1, 2, 3$ ) are defined as follows:

$$C_1 = \begin{pmatrix} 1 & 0 \\ 0 & 1 \end{pmatrix}, C_2 = \begin{pmatrix} \frac{1}{R_i^{NC}} & 0 \\ 0 & 0 \end{pmatrix}, C_3 = \begin{pmatrix} 0 & \frac{1}{R_i^{NC}} \\ 0 & 0 \end{pmatrix}.$$

The steps to convert (11)–(13) into (32)–(35) are described in Appendix A. SDP has been proven effective to generate a tight lower bound for the minimum objective value of non-convex problems [30]. A disadvantage of SDP relaxations is that the computational cost grows rapidly with the problem's size; however, since a distributed solution will be adopted, the problem will be divided into a series of small SDP sub-problems that can be easily solved.

After the convex relaxation of the power flow and ESs constraints, the optimization problem for the microgrid operation scheduling is defined by the objective function (1) subject to constraints (2)–(10), (18)–(28), (30)–(35).

#### IV. PRICE-BASED COORDINATION OF ELECTRIC SPRINGS

The above optimization problem is formulated for a centralized solution in which the voltage settings for the ESs are determined by the MGCC and sent to the local controllers through a two-way communication infrastructure. This approach requires the smart loads to communicate to the MGCC complete information of cost function, constraints, hot water demand and SOTC. Therefore, a decomposition method is applied to decouple the optimization of the smart loads from the main problem. This decomposition results in an optimization problem to be solved by the MGCC and set of sub-problems to be solved by the ESs local controllers. In this way, the ESs voltage settings can be determined by the local controllers, preserving the customers' information private. An additional benefit of this approach is that the computational burden is shared between the MGCC and the ES local controllers.

From the centralized formulation it is observed that constraints (26), (27) and (32) couple the variables of the smart loads with the variables of the main problem. To decouple constraints (26) and (27), the iterative PCPM algorithm [24], [25] is applied, while for constraint (32) it is considered that the magnitude squared of the bus voltages  $V_{i,t}^{sqr}$ , obtained from the solution of the main problem, are communicated to the sub-problems at each iteration. A description of the PCPM algorithm is presented in Appendix B.

The architecture of the control system necessary for the price-based coordination strategy is shown in Fig. 4, where the information flow is represented by the dashed arrows. This corresponds to a centralized control architecture with a two-way communication infrastructure that links the local controllers only with the MGCC. The MGCC operates as a central coordinator that guides the local controllers' decisions through the broadcast of price/control signals. These signals are determined at the MGCC when solving the main problem formulated to optimize the microgrid operation schedule. They are sent to the ESs local controllers that respond by estimating the ESs voltage settings that result in the smart loads active and reactive power schedules that optimize the smart loads operation cost and customers comfort. Then, each ES local controller communicates the active and reactive power schedules to the MGCC, which actualizes the price/control signals. This process is repeated iteratively until convergence is found. Since the scheduling is determined one day in advance, a real-time communication channel is not necessary. The information sent from the MGCC to the local controllers corresponds to the price/control signals that include the Lagrangian multipliers associated with the active and reactive powers of the receiving buses and the estimated magnitude squared of the receiving bus voltages. The local controllers return to the MGCC the smart loads' active and reactive power schedules.

The iterative process is presented below.

##### 1) Initialization:

Set  $k \leftarrow 0$ . For each bus  $i$  with ES and for each time interval  $t$ , the local controller arbitrarily chooses the initial  $P_{i,t}^{nc,k}$  and  $Q_{i,t}^{es,k}$  and communicate them to the MGCC. In parallel, the MGCC arbitrarily chooses the initial  $P_{i,t}^{cl,k}$ ,  $P_{i,t}^{g,k}$ ,  $P_{i,t}^{w,k}$ ,  $p_{i,t}^k$ ,

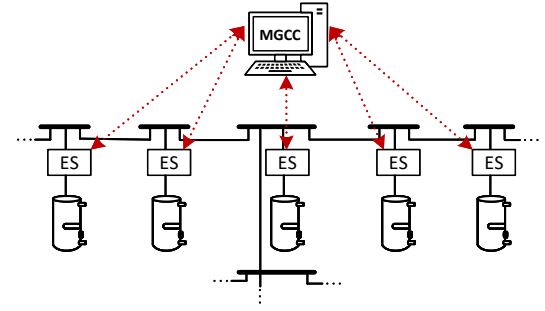


Fig. 4. Architecture of the ESs control system.

$Q_{i,t}^{gd,k}$ ,  $Q_{i,t}^{cl,k}$ ,  $q_{i,t}^k$  and two virtual control signals  $\hat{\mu}_{i,t}^k$  and  $\hat{\lambda}_{i,t}^k$  for each bus  $i$  and time interval  $t$ . The control signals  $\hat{\mu}_{i,t}^k$  and  $\hat{\lambda}_{i,t}^k$  are the Lagrangian multipliers associated, respectively, with the active and reactive power at bus  $i$  and time interval  $t$ .

##### 2) Predictor step:

The MGCC calculates the control signals  $\hat{\mu}_{i,t}^k$  and  $\hat{\lambda}_{i,t}^k$ , and communicates them to the local controllers of ESs.  $\hat{\mu}_{i,t}^k$  and  $\hat{\lambda}_{i,t}^k$  are calculated as follows:

$$\hat{\mu}_{i,t}^k := \mu_{i,t}^k + \gamma(P_{i,t}^{cl,k} + P_{i,t}^{nc,k} - P_{i,t}^{g,k} - P_{i,t}^{w,k} - p_{i,t}^k) \quad (36)$$

$$\hat{\lambda}_{i,t}^k := \lambda_{i,t}^k + \gamma(Q_{i,t}^{cl,k} + Q_{i,t}^{es,k} - Q_{i,t}^{g,k} - q_{i,t}^k) \quad (37)$$

where,  $\gamma$  is a positive constant. In this work,  $\hat{\mu}_{i,t}^k$  represents the energy price charged to the smart loads. It is assumed that the smart loads are not charged for their reactive power output because the control of the active power depends on the injection of reactive power by the ESs. Therefore,  $\hat{\lambda}_{i,t}^k$  does not represent a price.

##### 3) MGCC optimization:

The MGCC solves the following problem:

$$\begin{aligned} \min \quad & \sum_{t \in \Omega_t} \left( \sum_{i \in \Omega_b} \left( C^g(P_{i,t}^g) + C^w(P_{i,t}^w) + C^{cl}(P_{i,t}^{cl}) \right) + \right. \\ & \left. \alpha^b \sum_{ij \in \Omega_{ij}} r_{ij} I_{ij}^{sqr} \right) + (\hat{\mu}^k)^\top (P^{cl} - P^g - P^w - p) + \\ & (\hat{\lambda}^k)^\top (Q^{cl} - Q^g - q) + \frac{1}{2\gamma} \|P^{mg} - P^{mgk}\| + \\ & \frac{1}{2\gamma} \|Q^{mg} - Q^{mgk}\| \\ \text{s.t.} \quad & (2) - (10), (24), (25), (28), (30), (31) \end{aligned}$$

where  $P^{cl} := \text{vec}(P_{i,t}^{cl}, i \in \Omega_b, t \in \Omega_t)$ ,  $P^g := \text{vec}(P_{i,t}^g, i \in \Omega_b, t \in \Omega_t)$ ,  $P^w := \text{vec}(P_{i,t}^w, i \in \Omega_b, t \in \Omega_t)$ ,  $p := \text{vec}(p_{i,t}, i \in \Omega_b, t \in \Omega_t)$ ,  $Q^{cl} := \text{vec}(Q_{i,t}^{cl}, i \in \Omega_b, t \in \Omega_t)$ ,  $Q^g := \text{vec}(Q_{i,t}^g, i \in \Omega_b, t \in \Omega_t)$ , and  $q := \text{vec}(q_{i,t}, i \in \Omega_b, t \in \Omega_t)$  are column vectors whose elements are, respectively, the critical load active power, diesel generator active power, wind generator active power, net active power, critical load reactive power, diesel generator reactive power and net reactive power at each bus  $i$  and time interval  $t$ .  $\hat{\mu}^k := \text{vec}(\hat{\mu}_{i,t}^k, i \in \Omega_b, t \in \Omega_t)$  and  $\hat{\lambda}^k := \text{vec}(\hat{\lambda}_{i,t}^k, i \in \Omega_b, t \in \Omega_t)$  indicate the vectors of control signals;  $P^{mg} := \text{vec}(P^{cl}, P^g, P^w, p)$  and  $Q^{mg} := \text{vec}(Q^{cl}, Q^g, q)$  indicate the vectors of variables of the problem; and  $P^{mgk} := \text{vec}(P^{cl,k}, P^g,k, P^w,k, p^k)$

and  $Q^{mg^k} := \text{vec}(Q^{cl^k}, Q^{g^k}, q^k)$  indicate the vectors of optimal values obtained in the previous iteration. The optimal  $P^{mg^*}$  and  $Q^{mg^*}$  obtained from the optimization are set as  $P^{mg^{k+1}}$  and  $Q^{mg^{k+1}}$ , respectively. The MGCC communicates the values of the magnitude squared of the voltage magnitude  $V_{i,t}^{sqr^k}$  to the local controllers

#### 4) ES local controller optimization:

The local controller of each ES solves the following problem:

$$\begin{aligned} \min \sum_{i \in \Omega_b} \sum_{t \in \Omega_t} C^{mc} (SC_{i,t}) + (\hat{\mu}_i^k)^\top P_i^{nc} + (\hat{\lambda}_i^k)^\top Q_i^{es} + \\ \frac{1}{2\gamma} \left\| P_i^{nc} - P_i^{nc^k} \right\| + \frac{1}{2\gamma} \left\| Q_i^{es} - Q_i^{es^k} \right\| \\ \text{s.t.} \\ C_1 \bullet X_{i,t} - V_{i,t}^{sqr^k} = 0, \\ (18) - (23), (33) - (35) \end{aligned} \quad (38)$$

where,  $\hat{\mu}_i^k := (\hat{\mu}_{i,t}^k, t \in \Omega_t)$ ,  $\hat{\lambda}_i^k := (\hat{\lambda}_{i,t}^k, t \in \Omega_t)$ ,  $P_i^{nc} := (P_{i,t}^{nc}, t \in \Omega_t)$ ,  $Q_i^{es} := (Q_{i,t}^{es}, t \in \Omega_t)$ ,  $P_i^{nc^k} := (P_{i,t}^{nc^k}, t \in \Omega_t)$  and  $Q_i^{es^k} := (Q_{i,t}^{es^k}, t \in \Omega_t)$ . The optimal  $P_i^{nc^*}$  and  $Q_i^{es^*}$  obtained from the optimization are set as  $P_i^{nc^{k+1}}$  and  $Q_i^{es^{k+1}}$ , respectively. The local controllers of ESs communicate  $P_i^{nc^{k+1}}$  and  $Q_i^{es^{k+1}}$  to the MGCC.

#### 5) Corrector step:

The MGCC updates  $\mu_{i,t}^{k+1}$  and  $\lambda_{i,t}^{k+1}$  as follows:

$$\mu_{i,t}^{k+1} := \mu_{i,t}^k + \gamma (P_{i,t}^{cl^{k+1}} + P_{i,t}^{nc^{k+1}} - P_{i,t}^{g^{k+1}} - P_{i,t}^{w^{k+1}} - p_{i,t}^{k+1}) \quad (39)$$

$$\lambda_{i,t}^{k+1} := \lambda_{i,t}^k + \gamma (Q_{i,t}^{cl^{k+1}} + Q_{i,t}^{es^{k+1}} - Q_{i,t}^{g^{k+1}} - q_{i,t}^{k+1}) \quad (40)$$

Set  $k \leftarrow k + 1$ , and repeat steps 2 – 4 until convergence.

The termination condition adopted here is to stop when  $\left| P_{i,t}^{cl^k} + P_{i,t}^{nc^k} - P_{i,t}^{g^k} - P_{i,t}^{w^k} - p_{i,t}^k \right|$  and  $\left| Q_{i,t}^{cl^k} + Q_{i,t}^{es^k} - Q_{i,t}^{g^k} - q_{i,t}^k \right|$  are less than a specified tolerance.

## V. CASE STUDIES

To evaluate the performance of the proposed ESs coordination strategy, simulation results were obtained from a real microgrid in Guangdong province, China, [25]. This section first presents the technical data and specifications of the microgrid, DG, CLs and smart loads. Then, the results of case studies are presented to demonstrate the performance of the proposed strategy to optimize the microgrid and smart loads operation.

### A. Technical data and specifications

The configuration of the microgrid is shown in Fig. 5. The microgrid operates in islanded mode with a nominal voltage of 10 kV. CLs are represented with arrows with the peak active demand shown below. The total CLs active and reactive peak demands are 7.8 MW and 3.7 MVar, respectively. Wind-based DG is installed at buses 13 and 14 with a rated capacity of 2.75 MW each. It is considered that wind-based DG operates at unity power factor. Diesel generators are installed at buses 1 and 9 with a rated capacity of 3 MW and 2 MW,

respectively, and they are considered to provide reactive power limited to the capability curve. The ramping ability of the diesel generators is set to 30% of its rated power capacity ( $R_i^{max} = 0.3P_i^{g,max}$ ).

Smart loads composed of EWHs and ESs are located at buses 2, 7, 8 and 12. All EWHs have identical thermal storage capacity and peak hot water demand equivalent to 1500 kWh and 500 kW, respectively, calculated assuming an inlet water temperature of 20°C ( $T^l = 20^\circ\text{C}$ ), a set temperature of 65°C ( $T^u = 65^\circ\text{C}$ ), and ambient temperature of 20°C ( $T^a = 20^\circ\text{C}$ ) [14]. The power rating of all EWHs is 250 kW with 95% heating efficiency. The minimum and maximum voltages at all buses are limited to 0.95 p.u. and 1.05 p.u., respectively. The parameters of the diesel generators cost function are set to  $\alpha_i^g = 10$ ,  $\beta_i^g = 70$  and  $v_i^g = 20$  [25]. These parameters describe the diesel generator fuel cost curve and vary depending on the specific generator and operation conditions [31], [32]. The parameters of the cost functions of wind spillage, load shedding, and energy losses are set to  $\alpha_i^w = 12.5$ ,  $\alpha_i^{cl} = 250$ , and  $\alpha_i^p = 50$ , respectively [15]. These values can be different depending on specific regulations, agreements, and energy prices [33]. The parameters of the NCLs cost function are set to  $\delta_i = 0.5$  and  $\alpha_i^{nc} = 15$ . Setting  $\delta_i = 0.5$  implies penalization of SOTCs below 50% of the maximum value. The value of  $\gamma$  is set to 0.75 [25]. The normalized profiles of CL demand, hot water demand and wind power availability with one hour resolution used in the simulations are shown in Fig. 6. It is assumed the same variability of CL demand, hot water demand and wind power availability in all buses of the microgrid.

The model of the problem corresponding to the MGCC was implemented in the modeling language AMPL and solved using the commercial solver Knitro. The sub-problems corresponding to the ES local controllers were solved using CVX, a package for specifying and solving convex programs [34], [35]. Simulations were carried out in a computer with a processor Intel Core i7-6700HQ and 8 GB of RAM. The solution time for the complete problem was 219 seconds, which is within the acceptable time for day-ahead scheduling. Convergence was reached after 26 iterations, requiring for each iteration an average of 0.4 seconds to solve the problem corresponding to the MGCC and 0.65 seconds to solve the sub-problem corresponding to each ES local controller. The total solution time was obtained solving the sub-problems sequentially; however, in a practical implementation these sub-problems can be solved in parallel by the ES local controllers, which reduces the solution time.

### B. Load shifting effect of smart loads

To compare the results obtained with the proposed strategy, a case without ESs is defined. Without ES, the EWHs are operated according to an on/off control strategy in which the heating element is turned on and off when the SOTC reaches a lower and upper threshold, respectively. The power profiles obtained for the cases without ESs and with ESs operated according to the proposed strategy are shown in Fig. 7 and Fig. 8, respectively. When EWHs are considered

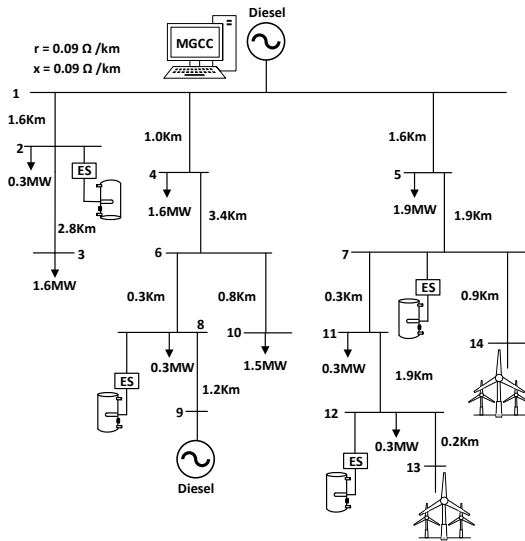


Fig. 5. Topology of the microgrid.

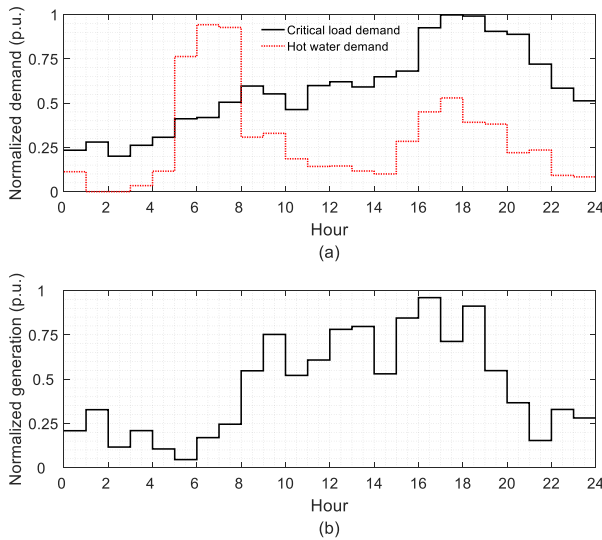


Fig. 6. Predicted profiles of a) Critical load demand and hot water demand, and b) wind power generation.

as non-flexible loads, there is energy generation surplus in the microgrid, which is relieved by spilling 3.7 MWh of wind energy. As shown in Fig. 7, most wind spillage occurs at hours 16-17 and 23-24 due to the rapid increase in the wind-based DG power availability, the insufficient ramping ability of the diesel generators, and the zero consumption of the EWHs. In addition, 1 MWh of CL is shed at hours 20-21 when the EHWs are turned on and the ramping up ability of the diesel generators cant follow the rapid decrease in the wind-based DG power output. With the flexibility introduced by the ESs, it is possible to shift the EWHs consumption to accommodate all the wind energy and avoid CL shedding as shown in Fig. 8. In this case, the ESs support the ramping ability of diesel generators to follow the variations of wind-based DG power output and CL demand.

The energy prices broadcast to the smart loads to coordinate their demand response are shown in Fig. 9. The energy prices are determined for the smart loads to adjust their consumption and help the diesel generators to balance demand and

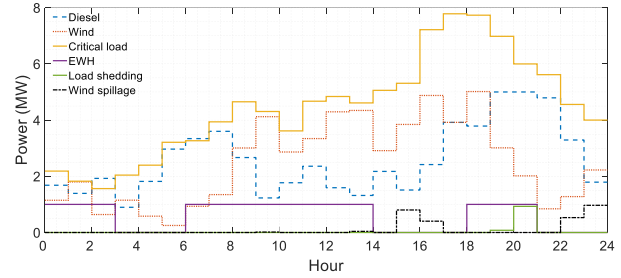


Fig. 7. Power schedules without electric springs.

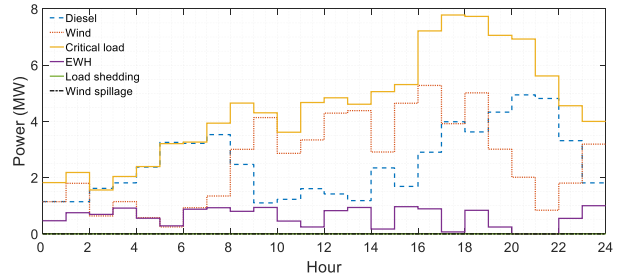


Fig. 8. Power schedules with electric springs.

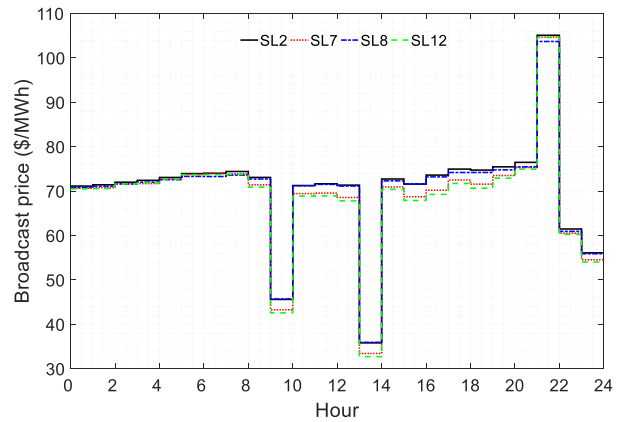


Fig. 9. Price signals sent to smart loads.

generation in an economic way. Rapid ramping ups of wind-based DG power output to values near the CL consumption at hours 10 and 14 lead to dips in energy prices that incentivize the consumption of smart loads as shown in Fig. 9. On the other hand, the smart load consumption at hour 22 is heavily penalized with a large energy price to compensate for the sharp decrease in wind-based DG power production and a relatively large CL consumption.

The SOTCs of the EWHs during the scheduling period for the case with ESs are shown in Fig. 10. It is observed that the smart loads consumption schedule fails to maintain the SOTC above the defined limit only at hours 8-9 due to the peak hot water demand and hours 20-23 due to high hot water demand and high energy prices. By assigning a higher value to the coefficient of the smart loads cost function it is possible to maintain the SOTC above 50%; however, at the expense of paying higher prices for the energy consumption. The operation costs for the microgrid operating without and with ESs are \$4744.93 and \$4361.69, respectively, which indicates a reduction of 8.10% when ESs are available. On the other hand, ESs allows reducing the payments the smart

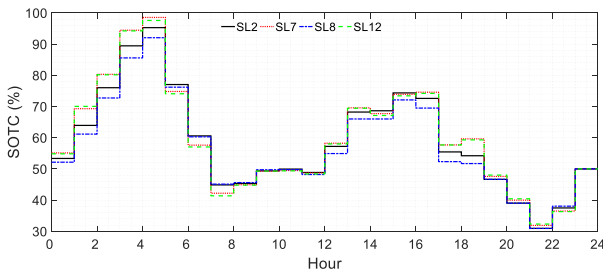


Fig. 10. State of thermal charge of electric water heaters.

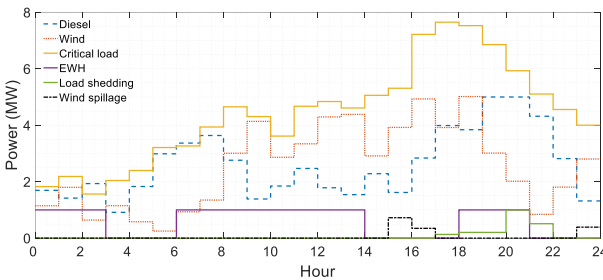


Fig. 11. Power schedules without electric springs for the scenario with longer lines.

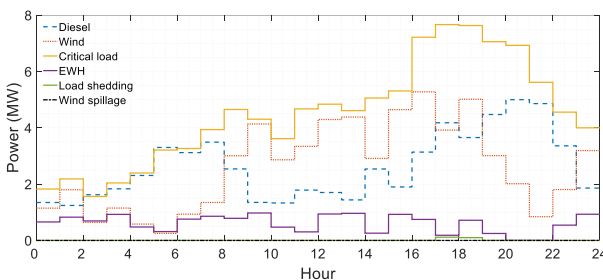


Fig. 12. Power schedules with electric springs for the scenario with longer lines.

loads made for energy consumption from \$1191.18 to \$957.67, which represents a reduction of 19.60%.

### C. Voltage regulation effect of smart loads

To test the performance of the proposed strategy to maintain the voltage levels supplied to CLs within acceptable bounds, the line lengths are multiplied by five. With longer lines, larger voltage deviations from the nominal value are expected to occur. The power profiles for the cases without and with ESs are shown in Fig. 11 and Fig. 12, respectively. Fig. 13 shows the voltage profiles of four representative buses in the microgrid (including the buses with the highest and lowest voltage levels) for the cases without and with ESs. Without ESs, 1.46 MWh of wind energy is spilt and 2.05 MWh of CL is shed to balance demand and generation and avoid voltage limit violations. Load shedding is necessary at bus 3 during the peak CL demand hours to avoid undervoltages as can be seen from Fig. 11 and Fig. 13(a). With ESs, wind spillage and load shedding are reduced to zero and 0.21 MWh, respectively. In this case, the ES at bus 2 reduces the EWH consumption during the peak CL demand hours to help avoid undervoltages at bus 3.

The energy prices to which the smart loads respond are shown in Fig. 14. In this scenario, the energy prices broadcast

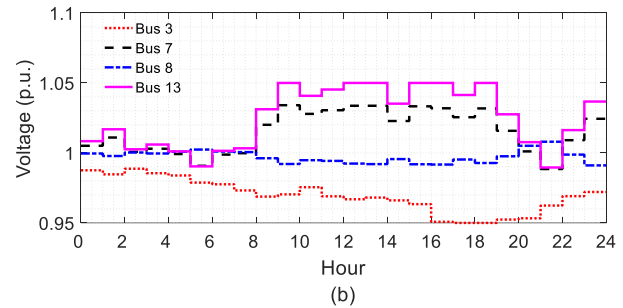
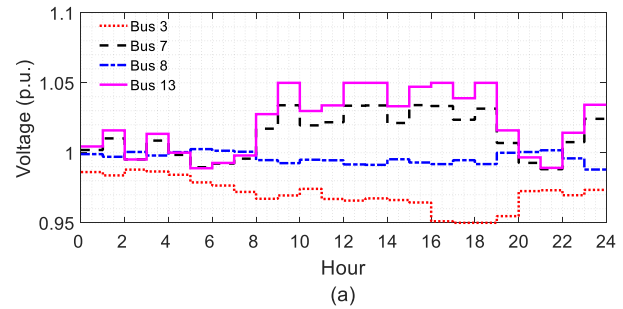


Fig. 13. Microgrid voltage profiles for the cases a) without ESs and b) with ESs.

to smart loads vary according to the location in the microgrid to promote a demand response that helps to maintain feasible voltage levels. Lower energy prices are delivered to smart loads at buses 7 and 12 between hours 9 and 20 to incentivize a higher energy consumption and avoid overvoltages in the section of the microgrid where wind-based DG is installed. From Fig. 13(b) it is observed that the voltage at bus 13 (the most distant bus) is less or equal to 1.05 p.u. during the period with higher wind-based DG power output (hours 9-20). On the other hand, the energy price charged to the smart load at bus 2 is significantly increased at the peak CL demand hours (hours 18 and 19) to discourage the energy consumption and avoid undervoltages at bus 3. Figure 13 illustrates the voltage profile at bus 3, where low voltage levels are obtained due to the absence of DG in that section of the microgrid and the large CL served.

The SOTCs of the EWHs for the case with ESs is shown in Fig. 15. A lower SOTC is obtained at hour 8 for the EWHs at buses 7 and 12 because their energy consumption is shifted to the period between hours 9 and 17 when the energy price is low. Conversely, the EWH at bus 2 has a higher SOTC between hours 14 and 17 because hot water is stored to supply the hot water demand during the period between hours 18 and 19 when the energy price is high.

When the length of the lines in the microgrid is increased, the operation cost for the cases without and with ESs increases to \$5016.72 and \$4596.40, respectively. The greater operation cost is due to the need to shed CL to avoid undervoltages at bus 3. The cost of energy for the smart loads changes to \$1232.50 and \$896.35 for the cases without and with ESs, respectively.

### D. Microgrid with solar PV generation

The impact of introducing solar PV generation in the microgrid on the performance of the proposed strategy was

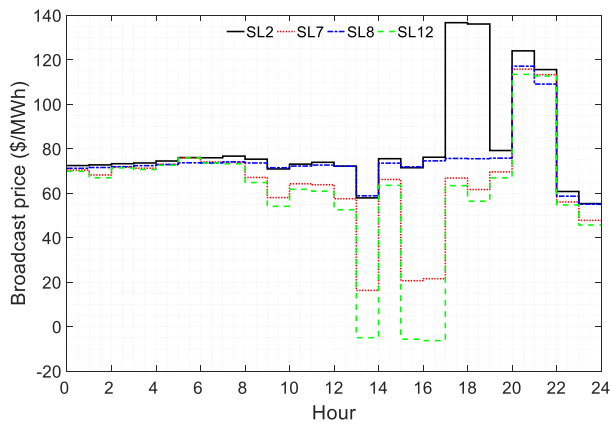


Fig. 14. Price signals sent to smart loads for the scenario with longer lines.

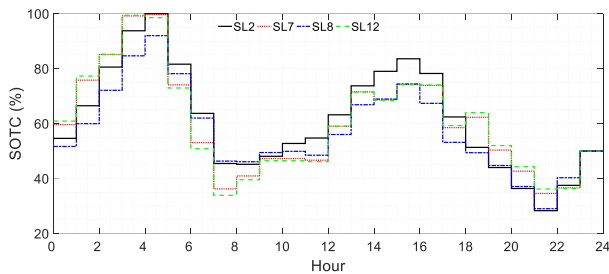


Fig. 15. State of thermal charge of electric water heaters for the scenario with longer lines.

evaluated by replacing the wind generator at bus 13 with a solar PV generator with the same rated capacity. The model used for solar PV generation is analogous to that used for wind generation [i.e., (6) and (7)] with the difference that the generation profile was changed to follow the solar PV generation availability. Tests were performed on the microgrid with the original length of lines, and the power profiles for the cases without and with ESs are shown in Fig. 16 and Fig. 17, respectively. Without ESs, 0.6 MWh of wind energy and 0.9 MWh of solar energy are spilt. From Fig. 16, it is observed that most solar energy is spilt at the hours with peak generation availability even when the ESs are turned on. In addition, a significant amount of CL equivalent to 5.7 MWh is shed when there is no solar PV generation. The active participation of ESs allows to reduce the wind energy spillage, solar energy spillage, and CL shedding to 0 MWh, 0.56 MWh, and 2.3 MWh, respectively. The microgrid operating cost for the cases without and with ESs is \$6676.53 and \$5992.47, respectively, which represents a 10.25% saving for the case with ESs. The cost of energy for the smart loads for the cases without and with ESs is \$1377.73 and \$887.10, respectively. This represents a cost saving of 35.61% for the case with ESs.

### E. Convergence performance evaluation

To decompose the centralized optimization problem defined in section II, two approximations were introduced. First, the non-convex constraints in the model were relaxed by using the procedure described in section III. Second, to decouple constraint (34) in section IV, it was assumed that the MGCC passes the magnitude squared of the bus voltage to the local

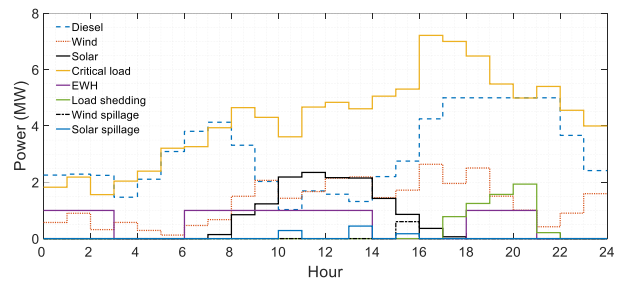


Fig. 16. Power schedules without electric springs in microgrid with solar PV generation.

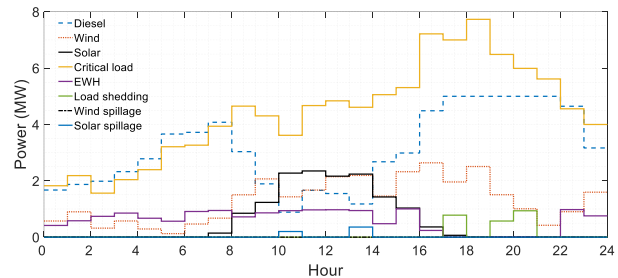


Fig. 17. Power schedules with electric springs in microgrid with solar PV generation.

controllers at each iteration, and the objective functions of the optimization problems at the MGCC and local controllers were not augmented with the terms that corresponds to that constraint. Ideally, if the convex relaxation were exact, the application of the pure PCPM algorithm to the relaxed problem will converge to the optimal solution of the non-convex problem. To test the performance of the adopted approximations, the non-convex centralized problem was solved for the case of the microgrid with long lines and wind-based DG using the commercial solver Knitro. The values obtained for the microgrid operation cost and the smart loads energy cost were \$4626.41 and \$887.04, respectively. This represents a difference of 0.65% and 1.05% with respect to the values obtained with the proposed decomposed approach.

## VI. CONCLUSION

In this paper, a smart pricing strategy was proposed to coordinate the operation of multiple ESs distributed in microgrids. This strategy was designed for the day-ahead operation scheduling of islanded microgrids that seek to optimize their operation cost taking into account the flexibility of smart loads composed of ESs connected to EWHs. Smart loads were modeled as rational agents that adjust their power schedules in response to price/control signals broadcast from the MGCC to optimize their own objectives. The MGCC determines the price/control signals when scheduling the power flows in the microgrid in a way that minimizes the microgrid operation cost when smart loads participate in demand side management. The coordination strategy was based on an optimization algorithm that iteratively solves the MGCC optimization problem and the local controllers optimization problems.

Simulation results showed that the utilization of ESs coordinated through the proposed strategy reduced the microgrid operation cost by 8.10% and the smart loads energy cost by 19.60% when compared with the case without ESs. The

control/price signals broadcast to the local controllers of ESs were effective in promoting power schedules of smart loads that contributed to reduce the wind spillage and the CL shedding. In addition, it was ensured the supply of hot water demand while maintaining a reserve of hot water in the tank for emergency situations. The effectiveness of the proposed strategy to maintain adequate bus voltage levels was also evaluated. Results showed that the participation of ESs contributed to avoid overvoltages and undervoltages requiring less CL shedding and wind spillage than the case without ESs. Besides economic benefits, the proposed strategy ensures the smart loads to maintain their information private. As future work, demand and generation uncertainties will be considered in the model.

## APPENDIX A

### SDP RELAXATION OF THE ES MODEL

In this work, SDP relaxation is used to convexify constraints (11)-(13), which are repeated here without the indices  $i$  and  $t$  to facilitate the readability.

$$V^{nc^2} + V^{es^2} = V^{sqr}, \quad (41)$$

$$P^{nc} = \frac{V^{nc^2}}{R^{nc}}, \quad (42)$$

$$Q^{es} = \frac{V^{es}V^{nc}}{R^{nc}}. \quad (43)$$

Defining the vector  $\mathbf{Y} := [V^{nc} \ V^{es}]^\top$ , (41)-(43) can be expressed as follows:

$$\mathbf{Y}^\top \mathbf{C}_1 \mathbf{Y} - V^{sqr} = 0, \quad (44)$$

$$\mathbf{Y}^\top \mathbf{C}_2 \mathbf{Y} - P^{nc} = 0, \quad (45)$$

$$\mathbf{Y}^\top \mathbf{C}_3 \mathbf{Y} - Q^{es} = 0, \quad (46)$$

where,  $\mathbf{C}_n$  ( $n = 1, 2, 3$ ) are coefficient matrices defined as follows:

$$\mathbf{C}_1 = \begin{pmatrix} 1 & 0 \\ 0 & 1 \end{pmatrix}, \mathbf{C}_2 = \begin{pmatrix} \frac{1}{R_i^{nc}} & 0 \\ 0 & 0 \end{pmatrix}, \mathbf{C}_3 = \begin{pmatrix} 0 & \frac{1}{R_i^{nc}} \\ 0 & 0 \end{pmatrix}.$$

The terms  $\mathbf{Y}^\top \mathbf{C}_n \mathbf{Y}$  in (44)-(46) can be expressed as  $\mathbf{C}_n \mathbf{Y} \mathbf{Y}^\top$ , which in turn can be expressed as  $\mathbf{C}_n \bullet \mathbf{X} := \sum_{k=1}^2 \sum_{l=1}^2 C_{n,k,l} X_{k,l}$ . This results in the following formulation:

$$\mathbf{C}_1 \bullet \mathbf{X} - V^{sqr} = 0, \quad (47)$$

$$\mathbf{C}_2 \bullet \mathbf{X} - P^{nc} = 0, \quad (48)$$

$$\mathbf{C}_3 \bullet \mathbf{X} - Q^{es} = 0, \quad (49)$$

$$\mathbf{X} = \mathbf{Y} \mathbf{Y}^\top. \quad (50)$$

Constraint (50) establishes that  $\mathbf{X} = \mathbf{Y} \mathbf{Y}^\top$  is a symmetric rank-1 positive semidefinite matrix [29]. By relaxing the rank-1 constraint, the problem is turned into a SDP program in the matrix variable  $\mathbf{X}$ . Therefore, constraint (50) is replaced by  $X_{i,t} \geq 0$ , which indicates that  $\mathbf{X}$  must be positive semidefinite. Constraints (47)-(49) are linear functions of the matrix variable  $\mathbf{X}$  whose elements are  $X_{k,l}$  ( $k = 1, 2, l = 1, 2$ ).

## APPENDIX B

### THE PCPM ALGORITHM

The PCPM algorithm is used in this work to decouple the optimization of the smart loads from the main problem. This algorithm was first introduced in [24] and is applied to solve convex optimization problems with separable structure of the form:

$$\min_{\mathbf{x}, \mathbf{y}} f(\mathbf{x}) + g(\mathbf{y}) \quad (51)$$

$$\text{s.t. } \mathbf{A}\mathbf{x} + \mathbf{B}\mathbf{y} = \mathbf{c} \quad (52)$$

The above is a generic form in which many convex problems can be formulated [24], [36]. Defining  $\mathbf{z}$  as the Lagrangian multiplier associated with constraint (52), the steps of the PCPM algorithm can be written as follows.

- 1) Set  $k \leftarrow 0$  and choose  $(\mathbf{x}^0, \mathbf{y}^0, \mathbf{z}^0)$  arbitrarily.
- 2) Compute  $\hat{\mathbf{z}}^k := \mathbf{z}^k + \gamma (\mathbf{A}\mathbf{x}^k + \mathbf{B}\mathbf{y}^k - \mathbf{c})$  where  $\gamma > 0$ .
- 3) Solve

$$\mathbf{x}^{k+1} = \arg \min_{\mathbf{x}} \left\{ f(\mathbf{x}) + \langle \hat{\mathbf{z}}^k, \mathbf{A}\mathbf{x} \rangle + \frac{1}{2\gamma} \|\mathbf{x} - \mathbf{x}^k\|^2 \right\},$$

$$\mathbf{y}^{k+1} = \arg \min_{\mathbf{y}} \left\{ g(\mathbf{y}) + \langle \hat{\mathbf{z}}^k, \mathbf{B}\mathbf{y} \rangle + \frac{1}{2\gamma} \|\mathbf{y} - \mathbf{y}^k\|^2 \right\},$$

where  $\langle \cdot, \cdot \rangle$  denotes the inner product.

- 4) Compute  $\mathbf{z}^{k+1} := \mathbf{z}^k + \gamma (\mathbf{A}\mathbf{x}^{k+1} + \mathbf{B}\mathbf{y}^{k+1} - \mathbf{c})$ .
- 5)  $k \leftarrow k + 1$ , and go to step 2 until convergence is found.

The PCPM algorithm performs two proximal steps in the Lagrangian multiplier, the predictor step 1 and the corrector step 4, and one proximal step 3 for the primal problem. This algorithm globally converges at a linear rate to an optimal primal-dual solution for a small enough step size  $\gamma$  provided that the problem (51), (52) is convex and has optimal solution [24].

## REFERENCES

- [1] S. Y. Hui, C. K. Lee, and F. F. Wu, "Electric springs a new smart grid technology," *IEEE Trans. Smart Grid*, vol. 3, no. 3, pp. 1552–1561, 2012.
- [2] X. Luo, Z. Akhtar, C. K. Lee, B. Chaudhuri, S.-C. Tan, and S. Y. R. Hui, "Distributed voltage control with electric springs: Comparison with statcom," *IEEE Transactions on Smart Grid*, vol. 6, no. 1, pp. 209–219, 2015.
- [3] X. Chen, Y. Hou, S. Tan, C. Lee, and S. Y. R. Hui, "Mitigating voltage and frequency fluctuation in microgrids using electric springs," *IEEE Trans. Smart Grid*, vol. 6, no. 2, pp. 508–515, 2015.
- [4] J. Soni and S. K. Panda, "Electric spring for voltage and power stability and power factor correction," *IEEE Trans. Ind. Appl.*, vol. 53, no. 4, pp. 3871–3879, 2017.
- [5] C. K. Lee and S. Y. Hui, "Reduction of energy storage requirements in future smart grid using electric springs," *IEEE Trans. Smart Grid*, vol. 4, no. 3, pp. 1282–1288, 2013.
- [6] T. Yang, K.-T. Mok, S.-S. Ho, S.-C. Tan, C.-K. Lee, and R. S. Y. Hui, "Use of integrated photovoltaic-electric spring system as a power balancer in power distribution networks," *IEEE Transactions on Power Electronics*, vol. 34, no. 6, pp. 5312–5324, 2019.
- [7] M. S. Javaid, A. Sabir, M. Abido, and H. Boucheqara, "Design and implementation of electric spring for constant power applications," *Electr. Power Syst. Res.*, vol. 175, p. 105884, 2019.
- [8] C. K. Lee, N. R. Chaudhuri, B. Chaudhuri, and S. Y. R. Hui, "Droop control of distributed electric springs for stabilizing future power grid," *IEEE Transactions on Smart Grid*, vol. 4, no. 3, pp. 1558–1566, 2013.
- [9] X. Chen, Y. Hou, and S. Y. R. Hui, "Distributed control of multiple electric springs for voltage control in microgrid," *IEEE Trans. Smart Grid*, vol. 8, no. 3, pp. 1350–1359, 2017.

- [10] Y. Yang, Y. Qin, S. Tan, and S. Y. R. Hui, "Reducing distribution power loss of islanded ac microgrids using distributed electric springs with predictive control," *IEEE Trans. Ind. Electron.*, vol. 67, no. 10, pp. 9001–9011, 2020.
- [11] L. Liang, Y. Hou, and D. J. Hill, "An interconnected microgrids-based transactive energy system with multiple electric springs," *IEEE Trans. Smart Grid*, vol. 11, no. 1, pp. 184–193, 2020.
- [12] L. Liang, H. Yi, Y. Hou, and D. J. Hill, "An optimal placement model for electric springs in distribution networks," *IEEE Trans. Smart Grid*, vol. 12, no. 1, pp. 491–501, 2021.
- [13] X. Luo, C. K. Lee, W. M. Ng, S. Yan, B. Chaudhuri, and S. Y. R. Hui, "Use of adaptive thermal storage system as smart load for voltage control and demand response," *IEEE Transactions on Smart Grid*, vol. 8, no. 3, pp. 1231–1241, 2017.
- [14] T. Chen, Y. Zheng, B. Chaudhuri, and S. Y. R. Hui, "Distributed electric spring based smart thermal loads for overvoltage prevention in lv distributed network using dynamic consensus approach," *IEEE Trans. Sustain. Energy*, vol. 11, no. 4, pp. 2098–2108, 2020.
- [15] L. Liang, Y. Hou, and D. J. Hill, "Enhancing flexibility of an islanded microgrid with electric springs," *IEEE Trans. Smart Grid*, vol. 10, no. 1, pp. 899–909, 2019.
- [16] J. Zhang, G. Ma, X. Lyu, M. Li, J. Xu, and X. Wu, "Research on scheduling control strategy of large-scale air conditioners based on electric spring," *Int. J. Electr. Power Energy Syst.*, vol. 124, p. 106398, 01 2021.
- [17] Y. Yan, Z. Chen, V. Varadharajan, M. J. Hossain, and G. E. Town, "Distributed consensus-based economic dispatch in power grids using the paillier cryptosystem," *IEEE Transactions on Smart Grid*, vol. 12, no. 4, pp. 3493–3502, 2021.
- [18] P. Samadi, A.-H. Mohsenian-Rad, R. Schober, V. W. S. Wong, and J. Jatskevich, "Optimal real-time pricing algorithm based on utility maximization for smart grid," in *2010 First IEEE International Conference on Smart Grid Communications*, 2010, pp. 415–420.
- [19] N. Li, L. Chen, and S. H. Low, "Optimal demand response based on utility maximization in power networks," in *2011 IEEE Power and Energy Society General Meeting*, 2011, pp. 1–8.
- [20] M. Arriaga, C. A. Cañizares, and M. Kazerani, "Northern lights: Access to electricity in canada's northern and remote communities," *IEEE Power Energy Mag.*, vol. 12, no. 4, pp. 50–59, 2014.
- [21] H. Xie, S. Zheng, and M. Ni, "Microgrid development in china: A method for renewable energy and energy storage capacity configuration in a megawatt-level isolated microgrid," *IEEE Electrification Mag.*, vol. 5, no. 2, pp. 28–35, 2017.
- [22] A. Anderson, P. Loomba, I. Oranjaka, J. Numfor, S. Saha, S. Janko, N. Johnson, R. Podmore, and R. Larsen, "Empowering smart communities: Electrification, education, and sustainable entrepreneurship in ieeec smart village initiatives," *IEEE Electrification Mag.*, vol. 5, no. 2, pp. 6–16, 2017.
- [23] S. M. Nosratabadi, R.-A. Hooshmand, and E. Gholipour, "A comprehensive review on microgrid and virtual power plant concepts employed for distributed energy resources scheduling in power systems," *Renewable and Sustainable Energy Reviews*, vol. 67, pp. 341–363, 2017.
- [24] G. Chen and M. Teboulle, "A proximal-based decomposition method for convex minimization problems," *Mathematical Programming*, vol. 64, no. 1, pp. 81–101, 1994.
- [25] W. Shi, X. Xie, C. Chu, and R. Gadh, "Distributed optimal energy management in microgrids," *IEEE Trans. Smart Grid*, vol. 6, no. 3, pp. 1137–1146, 2015.
- [26] J. Kondoh, N. Lu, and D. J. Hammerstrom, "An evaluation of the water heater load potential for providing regulation service," *IEEE Trans. Power Syst.*, vol. 26, no. 3, pp. 1309–1316, 2011.
- [27] M. Baran and F. Wu, "Network reconfiguration in distribution systems for loss reduction and load balancing," *IEEE Transactions on Power Delivery*, vol. 4, no. 2, pp. 1401–1407, 1989.
- [28] L. Gan, N. Li, U. Topcu, and S. H. Low, "Exact convex relaxation of optimal power flow in radial networks," *IEEE Transactions on Automatic Control*, vol. 60, no. 1, pp. 72–87, 2015.
- [29] H. Wolkowicz, R. Saigal, and L. Vandenberghe, *Handbook of Semidefinite Programming*. Springer, Boston, MA, 2000.
- [30] S. Kim and M. Kojima, "Second order cone programming relaxation of nonconvex quadratic optimization problems," *Optimization Methods and Software*, vol. 15, no. 3–4, pp. 201–224, 2001.
- [31] A. J. Wood, B. F. Wollenberg, and G. B. Sheble, *Power generation, operation, and control*. Hoboken, NJ: Wiley, 2014.
- [32] M. Mobarra, M. Rezkallah, and A. Ilinca, "Variable speed diesel generators: Performance and characteristic comparison," *Energies*, vol. 15, no. 2, 2022.
- [33] P. Hallberg, "Active distribution system management a key tool for the smooth integration of distributed generation," *Eurelectric TF Active System Management*, vol. 2, no. 13, 2013.
- [34] M. Grant and S. Boyd, "CVX: Matlab software for disciplined convex programming, version 2.1," <http://cvxr.com/cvx>, mar 2014.
- [35] —, "Graph implementations for nonsmooth convex programs," in *Recent Advances in Learning and Control*. Springer-Verlag Limited, 2008, pp. 95–110.
- [36] R. T. Rockafellar, *Convex Analysis*. Princeton, NJ: Princeton University Press, 1970.